



Immobilization of esterase from *Bacillus subtilis* on Halloysite nanotubes and applications on dibutyl phthalate degradation

Esin Balci ^{a,b,*}, Emilio Rosales ^{a,**}, Marta Pazos ^a, Aysun Sofuoglu ^c,
Maria Angeles Sanromán ^a

^a CINTECX, Universidade de Vigo, Grupo de Bioingeniería y Procesos Sostenibles, Departamento de Ingeniería Química, Campus Lagoas-Marcosende, 36310 Vigo, Spain

^b Izmir Institute of Technology, Faculty of Engineering, Department of Environmental Engineering, 35430 Urla/Izmir, Turkey

^c Izmir Institute of Technology, Faculty of Engineering, Department of Chemical Engineering, 35430 Urla/Izmir, Turkey



ARTICLE INFO

Article history:

Received 4 January 2023

Received in revised form 5 March 2023

Accepted 14 March 2023

Available online 17 March 2023

Keywords:

Esterase

Dibutyl phthalate

Halloysite

Enzyme immobilization

Enzymatic degradation

ABSTRACT

Dibutyl phthalate (DBP) is one of the listed phthalic acid esters (PAEs) known as the priority toxicants which exhibit carcinogenic and teratogenic properties and is responsible for endocrine disruption. Therefore, its removal has become a matter to tackle with. In this work, the feasibility of DBP degradation by esterase and lipase enzymes obtained from various microorganisms and the immobilization of the most effective in a clayey material were investigated. Esterase from *Bacillus subtilis* exhibited the highest degradation efficiency reaching a complete degradation. Its immobilization onto halloysite nanotubes (HNTs) by adsorption method was studied by response surface methodology using a central composite design face-centered. The four selected factors that affect the HNT-enzyme composite generation were: pH, adsorption time, enzyme/HNT (E/H) ratio, and adsorption temperature, and the optimal conditions were determined (pH 7, time 360 min, E/H ratio 0.2, temperature 30°C). Consequently, the activity did not significantly decrease by immobilization, and the adsorption efficiency and relative activity were determined to be 73.15% and 82.7%, respectively. Besides, the immobilization enhanced thermal and storage stability. As for enzyme reusability, after 7 continuous cycles, the composite maintained almost 75% of its initial activity. Both the free enzyme (1 mg/mL) and the composite degraded 100 mg/L DBP with 100% efficiency and several byproducts were detected. Moreover, the composite could be reused for 7 cycles keeping a remarkable catalytic activity. Overall, this study indicated that the HNT-enzyme composite may be used as an effective candidate for remediation of the environmental media contaminated with DBP and other PAEs.

© 2023 The Author(s). Published by Elsevier B.V. This is an open access article under the CC BY-NC-ND license (<http://creativecommons.org/licenses/by-nc-nd/4.0/>).

1. Introduction

Over the past few decades, the number of synthetic chemicals found in pharmaceutical and manufacturing additives as well as metal, personal and household care products has increased to supply the needs of modern society. The production volume of phthalic acid esters (PAEs) is over 8 million metric tons per year in the world (Seyoum and Pradhan, 2019;

* Corresponding author at: Izmir Institute of Technology, Faculty of Engineering, Department of Environmental Engineering, 35430 Urla/Izmir, Turkey.

** Corresponding author.

E-mail addresses: esinbalci@iyte.edu.tr (E. Balci), emilirov@uvigo.es (E. Rosales).

Balci et al., 2022). PAEs are ubiquitous and recalcitrant compounds that can be released into the environment during their manufacturing and use. Thus, they are degraded slowly under natural conditions and accumulate in the air, surface water, wastewater, sediment, and soil over time (Scholz et al., 1997; Pirsabeheh and Zinatizadeh, 2009; Kong et al., 2018; Baloyi et al., 2021). Most PAEs can easily migrate to various water bodies and then enter a variety of aquatic organisms (Cao et al., 2018; Huang et al., 2021) and being accumulated in the food chain and cause health problems such as chronic health effects, cancer risks, and endocrine disruption. Additionally, they have significant adverse impacts on mammalian reproduction, development, and the nervous system (Wang et al., 2023). Among the various types of PAEs, dimethyl phthalate (DMP), diethyl phthalate (DEP), dibutyl phthalate (DBP), butyl benzyl phthalate (BBP), di-n-octyl phthalate (DnOP), diethyl hexyl phthalate (DEHP) have been categorized as priority pollutants by The United States Environmental Protection Agency (USEPA) and its counterparts in European Union countries.

Different available methods include photolysis and hydrolysis, however, biodegradation is considered safer, cleaner, and more environmentally friendly. Recently, there has been a significant increase in the use of enzymes in various industries such as biomedicine, food, and energy. The enzymes have a vital role to protect the environment (Moreira et al., 2020; Bilal et al., 2022). Hydrolase enzymes such as esterase and lipase are very effective on the ester bonds in the structure of PAEs (Sharma et al., 2019). There are several studies demonstrating that esterase from *Bacillus* sp. and lipase from *Candida cylindracea*, *Pseudomonas* sp. V21b and *Comamonas* sp. 51F exhibit the ability to degrade PAEs (Tanaka et al., 2000; Ding et al., 2015; Sungkeeree et al., 2017; Kumar et al., 2017). However, enzymes are relatively unstable losing their structural stability for the duration of any reaction and, thus, having a short catalytic lifetime (Brena et al., 2013; Sharma et al., 2021; Souza et al., 2022). The generation of a composite by immobilization of the enzyme enhances the kinetic and biochemical properties of enzymes enabling enzyme recycling and reuse and reducing its inhibition (Zhai et al., 2010; Monteiro et al., 2019; Cavalcante et al., 2021; Bilal et al., 2022). Adsorption is one of the simplest and most economical immobilization methods not requiring the use of chemicals and the generated composite can be reused multiple times (Sassolas et al., 2012). The choice of adequate support material is crucial and several alternatives have been proposed in the literature, including the most expensive activated carbon and nanoparticles or cheaper natural minerals (Kamble et al., 2012; Yeniova-Erpek et al., 2015). Among the natural minerals with high abundance (zeolite, hydrotalcite, or nanotubes), only zeolite and hydrotalcite are suitable for loading certain specific enzymes due to their limited pore diameters and surface areas. Materials with nano-scale structures can greatly enhance the active surface available for enzyme adsorption (Zhao et al., 2017). Halloysite nanotubes (HNTs) have a non-toxic, porous, and biocompatible structure being suitable materials for the composite. In comparison with other nano-scale materials, they are easily obtainable and much more cost-effective than carbon nanotubes (CNTs) (Zhai et al., 2010). Besides, materials with HNTs have high mechanical strength compared to those with kaolinites (Gass et al., 2015). HNTs are inorganic natural clay minerals with a large surface area consisting of two-layer aluminosilicates and have a length of between 400 and 1,000 nm. They have a negative outer surface containing silicon dioxide (SiO_2) with an outer diameter between 50 and 100 nm, and a positive inner surface of aluminum hydroxide ($\text{Al}(\text{OH})_3$) with a lumen diameter ranging between 15 and 20 nm (Tari et al., 1999; Yeniova-Erpek et al., 2015). The maintenance of the counter-charged surfaces of HNTs between pH 3 and 10 constitutes a selectivity for the immobilization of the charged molecule (Kamble et al., 2012). Besides, the most obvious difference between HNTs and other aluminosilicate minerals is that HNTs have a unique nanotubular structure and biocompatibility (Ferrari et al., 2017). Due to all these properties, HNTs appear to be a very attractive matrix for the immobilization of various molecules such as drugs, antiseptics, corrosion inhibitors, and proteins (Abdullayev et al., 2009; Patel et al., 2016; Tully et al., 2016; Rao et al., 2018). Immobilization on HNTs improves enzyme stability, activity, selectivity, and specificity, and prevents enzyme inhibition, thus making enzymes reusable in continuous reactors.

Central composite design (CCD) is a statistical experimental design technique used to optimize and model a response variable, typically in the context of engineering, chemistry, or other scientific fields. It enables the investigation of the covariance of variables (independent factors) to achieve the optimal response (dependent factor) with a minimal number of experiments (Monteiro et al., 2019). In this context, CCD of the response surface methodology (RSM) was applied to determine the optimum values of process variables for the immobilization of the enzyme to HNTs in this study.

So far, a few studies have focused on the degradation of PAEs in the presence of a hydrolase enzyme in the literature. However, there are no studies on the immobilization of a hydrolase enzyme obtained from bacteria on HNTs and its subsequent use in the degradation of PAEs. In this sense, the study may form the basis for the use of the immobilized enzyme to HNTs in various environmental compartments for the degradation of PAEs. Furthermore, the potential uses of the immobilized enzyme (environmental treatment, food, pharmaceutical, industrial sectors, etc.) may expand.

In the present study, firstly, the ability of commercial lipase and esterase enzymes to degrade DBP, which is one of the most widely used and produced PAEs, was investigated. The enzyme exhibiting the highest DBP degrading ability was immobilized onto HNTs generating a composite. Then, the optimal conditions for the immobilization were determined by CCD. Next, the biocompatibility between the enzyme and HNT in the composite was investigated and used to treat DBP. Finally, the generation of DBP metabolites and the reuse of the composite were investigated.

2. Material and methods

2.1. Materials

Pure halloysite (HNT) powder was provided by Esan, Eczacıbasi Industrial Raw Materials Company (Istanbul, Turkey). Esterase enzymes (esterase from *Bacillus subtilis* (EC 3.1.1.1; ≥ 10 U/mg) and *Bacillus stearothermophilus* (EC 3.1.1.1; ≥ 0.2

U/mg)) were obtained from Sigma-Aldrich and lipase enzymes (lipozyme CALB from *Candida Antarctica B.* (EC 3.1.1.3; 5,000 LU/g), lipozyme TL 100 L from *Thermomyces lanuginosus* (EC 3.1.1.3; 100 KLU/g), and palatase 20,000 L from *Rhizomucor miehei* (EC 3.1.1.3; 20,000 LU/g)) were purchased from Novozymes (Denmark). Bovine serum albumin (BSA, >99%), DBP (99%), Methanol (99.8% ACS reagent), Tween-80 and p-nitrophenyl acetate (pNPC-2, esterase substrate >98%) were purchased from Sigma-Aldrich. Other chemicals were of laboratory reagent grade and used without any further purification.

2.2. DBP degradation in the presence of free enzymes

To investigate the DBP degrading ability of free enzymes, a DBP solution (1,000 mg/L) was prepared in methanol. To increase the solubility of DBP in the solution, Tween-80 was used as a solubilizing agent. The reaction mixture (1 mL) consisted of 0.1 mL of the free enzyme (1 mg/mL), 0.1 mL of 1,000 mg/L DBP in methanol, 0.1 mL of Tween-80 (1%, v/v), and 0.7 mL of phosphate buffer (0.1 M, pH 7). The reaction mixture was incubated for 15 min under optimum conditions determined by the manufacturers. After incubation of the reaction mixtures for an interval of a specific time, the samples were collected. 1 N HCl was added to the collected samples at a rate of 10% (v/v) to stop the enzymatic reaction (Saito et al., 2010). All samples were filtered through a 0.22 μm PTFE syringe filter to remove particles prior to HPLC analysis.

2.3. Enzyme immobilization on HNT and optimization

2.3.1. HNT-enzyme composite

The enzyme immobilization by adsorption was conducted with minor modifications to the study of Wang et al. (2015). Firstly, an enzymatic solution (1 mg/mL) in which the selected enzyme was dissolved in sodium phosphate buffer (0.1 M, pH 7) and stirred well was prepared. Next, 1 ml of this solution was added to the HNTs with an Enzyme/HNTs (E/H) ratio of 0.2. The obtained suspensions were vortexed for 5 min and stirred at 150 rpm in an incubator shaker for 195 min. Then, the Enzyme-HNTs were sonicated for 30 min to eliminate the agglomeration of HNTs. They were centrifuged at 8,000 rpm for 10 min. The supernatant phase was collected and then the HNT pellets with enzyme were washed twice with the buffer (1 mL) to remove excess protein/unbounded enzyme. Following this, the supernatant and washing solutions were stored at 4 °C for the activity measurement and determination of protein concentration.

2.3.2. Optimization of the parameters for the immobilization procedure

The optimization of the parameters affecting the enzyme immobilization was carried out using the RSM and more specifically, a central composite design face-centered (CCDFC) was selected for this purpose. This design was developed using the Design-Expert software 8.00 (Stat-Ease Inc., Minneapolis, USA) to explore the impact of the selected independent variables on the immobilization process (pH, adsorption time, E/H ratio, and temperature). These variables were labeled as X_1 , X_2 , X_3 , and X_4 , respectively. The adsorption efficiency (%) and the specific enzyme activity (U/mg) were taken as responses Y_1 and Y_2 , respectively.

A CCDFC design 2^4 (2-levels-4 factors) was used to determine the optimum conditions of the variables considering the following ranges: pH (5–7), adsorption time (30–360 min), E/H ratio (0.02–0.2 mg enzyme/mg HNT), and temperature (20–40 °C). In the CCDFC, the number of experimental tests ($N=30$) was calculated using Eq. (1) with 2^n factorial runs, n axial runs, and n_c central points.

$$N = 2^n + 2n + n_c \quad (1)$$

The statistical analysis of the model was carried out using analysis of variance (ANOVA) with Design Expert[®] 8.0.0 software. This analysis included the Fisher's F test (overall model significance), its associated probability values, and the coefficient of determination R^2 which measures the goodness of fit of the regression model (Rosales et al., 2012). The responses were expressed using a quadratic polynomial regression model to describe the correlation between responses and independent variables. The model Eq. (2) is as follows:

$$Y = \beta_0 + \sum_{i=1}^n \beta_i X_i + \sum_{i=1}^n \beta_{ii} X_i^2 + \sum_{i=1}^n \sum_{j=1}^n \beta_{ij} X_i X_j + \varepsilon \quad (2)$$

where Y represents the response of dependent variables; X_i and X_j are the independent variables; β_0 , β_i , β_{ii} , and β_{ij} are the mathematical model constants, the linearity coefficient of i factor, the quadratic coefficient of i factor, and the interaction coefficient between factors (i and j), respectively; ε is an experimental uncertainty (error) that indicates the various sources variability.

2.4. Characterization analysis

Before and after the adsorption experiments, numerous analyses were conducted to determine both the structure and the structural changes in raw HNTs and HNT-enzyme composite. Before the characterization analysis, raw HNTs and HNT-enzyme composite were dried in a vacuum oven at 100 °C and 45 °C, respectively to eliminate their moisture content.

2.4.1. Structural characterization of the composite

The microstructure of HNTs was examined using an FEI QUANTA 250 FEG scanning electron microscopy (SEM) instrument-equipped secondary detector. To observe detailed surface characteristics of HNTs and HNT-enzyme composite, the analysis of transmission electron microscopy (TEM) was performed on MICRO JEOL JEM 1010 at 200 kV (Service of Electronic Microscopy, C.A.C.T.I., University of Vigo, Vigo, Spain). To determine the crystal structure of the HNTs, X-ray diffraction analysis (XRD) was carried out at $2\theta=3-80^\circ$ using the Philips Xpert Pro XRD analyzer at a scanning rate of $0.02^\circ/\text{min}$.

2.4.2. Nanotextural and chemical characterization of the composite

The nanotextural and chemical characterization was performed by Brunauer–Emmett–Teller (BET) analysis, Fourier transform infrared spectroscopy (FT-IR), and thermogravimetric analysis (TGA). BET was performed using Mikromeritics TriStar II Plus 3.00 to determine the surface area and micropore size distribution of HNTs and HNT-enzyme composite. FT-IR analysis was done using JASCO FT-IR 4100 (Jasco Inc., Easton, MD, USA) equipped with an attenuated total reflectance (ATR) accessory to examine functional groups in HNTs and HNT-enzyme composite between 4000 and 400 cm^{-1} . The samples were mixed with potassium bromide and pelletized. TGA was carried out using a Seteram thermogravimetric analyzer with a temperature range that started at room temperature and ended at 800°C at a heating rate of $10^\circ\text{C}/\text{min}$ under $20\text{ mL}/\text{min}$ N_2 atmosphere to record the weight change and to indicate the thermal stability and heat resistance of the HNTs and HNT-enzyme composite.

2.5. Degradation studies in presence of the HNT-enzyme composite

In degradation experiments conducted using immobilized enzyme, HNT-enzyme composite (5 mg) was taken in a glass tube. Then, the reaction mixture containing 0.1 mL of DBP (1,000 mg/L), 0.1 mL Tween-80 (1%, v/v) solution, and 0.8 mL of phosphate buffer (0.1 M, pH 7) was added to the glass tube. During 1h-periods, the samples were put into an incubator shaker to degrade 100 mg/L DBP. At the end of each cycle consisting of 1h-periods, the samples were collected. They were vortexed for 30 s and centrifuged at 5,000 rpm for 10 min. After centrifugation, the supernatant phase was collected, and 1 N HCl was added to the supernatant at a rate of 10% (v/v) to stop the enzymatic reaction. Then, the supernatant was filtered through a $0.22\ \mu\text{m}$ PTFE syringe filter to remove particulate material from the samples. It was stored at 4°C for further analysis. At the end of each cycle, the pellet phase with the enzyme was fed with the reaction mixture. The relative activity was calculated after each catalytic cycle according to Eq. (3). The first measured activity of the immobilized enzyme was assumed to be 100% (He et al., 2015).

$$\text{Relative activity (\%)} = \frac{\text{Activity at the end of } n\text{th cycle}}{\text{Activity at the end of 1st cycle}} \times 100 \quad (3)$$

2.6. Analytical procedures

2.6.1. Determination of the enzyme activity and protein concentration

The enzyme activity was determined by hydrolysis of pNPC-2 according to Tekedar and Sanli-Mohamed (2011). The assay mixture (1 mL) consisted of 0.8 mL phosphate buffer (0.1 M, pH 7), 0.1 mL of 0.5 mM pNPC-2 dissolved in acetonitrile, and 0.1 mL of enzyme solution (1 mg/mL). This solution was incubated at optimum temperature for 5 min and then used to determine the catalytic activity. The absorbance was spectrophotometrically measured at 400 nm. After the measurement of the absorbance, the activity calculation will be made according to the following Eq. (4).

$$\text{Enzyme activity (U/L)} = \frac{(\text{Absorbance at } 400\text{ nm}/\text{min}) \cdot (V_t) \cdot (\text{DF})}{(\epsilon) \cdot (V_e) \cdot (d)} \quad (4)$$

where V_t : Test volume (mL), DF: Dilution factor, ϵ : molar extinction coefficient of 4-nitrophenol at 400 nm, V_e : Volume of enzyme used (mL), d : Lightpath (1 cm).

One unit (U) of activity is defined as the amount of enzyme releasing $1.0\ \mu\text{mol}$ of 4-nitrophenol per minute at pH 7, optimum temperature, and using pNPC-2 as a substrate. The molar extinction coefficient of 4-nitrophenol in the buffer system is $17,215\ \text{M}^{-1}\ \text{cm}^{-1}$.

The protein concentration of the initial enzyme solution, supernatant, and washing solution was determined according to Bradford Method (Bradford, 1976). The amount of adsorbed enzyme was calculated based on a mass balance. Adsorption efficiency (%) and enzyme loading amount (mg/mg) were calculated based on the quantity of unadsorbed protein according to the following Eqs. (5)–(6):

$$\text{Ads. eff. (\%)} = \frac{\text{Initial protein amount} - (\text{protein amount in the supernatant and washing solution})}{\text{Initial protein amount}} \times 100 \quad (5)$$

$$\text{Load. amount} \left(\frac{\text{mg}}{\text{mg}} \right) = \frac{\text{Initial protein amount} - (\text{protein amount in the supernatant and washing solution})}{\text{mass of HNT}} \quad (6)$$

2.6.2. Enzyme stability and reusability tests

Enzyme stabilization is a key objective of enzyme immobilization, as it enables the preservation of enzyme activity against changing conditions and allows for enzyme reuse in multiple reaction cycles (Cruz-Ortiz et al., 2011).

To perform the thermal stability tests, free esterase and HNT-enzyme composite were incubated in phosphate buffer (0.1 M, pH = 7) at various temperatures ranging from 20 to 70 °C. Following incubation, the samples were collected. After cooling, the activity was measured in the presence of 0.5 mM pNPC-2 substrate.

For the storage stability tests, both free esterase and the HNT-enzyme composite were stored for 14 days. Aliquots were taken for a predetermined period of time to measure the enzyme activity using 0.5 mM pNPC-2 substrate.

The enzyme activity of the HNT-enzyme composite was measured to determine the reusability of the composite. The same sample was used repeatedly for 7 cycles of enzyme catalysis. In each cycle, the sample was incubated with 0.5 mM pNPC-2 dissolved in acetonitrile for 5 min at 30 °C. After incubation, the supernatant was separated to measure the enzyme activity. The difference between the enzyme activity of the sample before incubation and that of the supernatant after incubation was calculated for each cycle. The remaining activity was expressed as relative activity (%).

2.6.3. Determination of kinetic parameters

The kinetic parameters, including the V_{max} and K_m , of both free esterase and HNT-enzyme composite, were determined by measuring enzyme activity at various concentrations of pNPC-2 (0–50 mg/L). The Lineweaver–Burk plots were used to estimate the kinetic parameters.

2.6.4. Analysis of DBP and its metabolites

DBP concentrations were determined under a reversed-phase using an Agilent 1260 Infinity series HPLC-DAD equipped with a column ZORBAX Eclipse XDB C-8 column (5 μ m particle size, 150 mm \times 4.6 mm i.d.). The mobile phase consisting of acetonitrile:water (60:40, v/v) was used at a flow rate of 1 mL/min. For each injection, the volume taken from samples was 20 μ L. The analysis was carried out together with a UV detector (224 nm) at room temperature.

DBP metabolites were identified using a trapped ion-mobility spectrometry time-of-flight mass spectrometer (TIMS-TOF-MS) (Bruker Daltonics, Bremen Germany). Ionization was performed using an electrospray (ES) source with a voltage of 3.5 kV applied to the needle and an endplate offset of 500 V. Using both positive and negative scan modes, ES spectral data was obtained. Data was acquired using Bruker Otof Control Software version 5.1 and processed with the Data analysis software version 5.1 from Bruker Daltonics.

3. Results and discussion

3.1. Determination of the most suitable enzyme for DBP degradation

Before enzymatic degradation experiments, the optimal temperature for each enzyme was evaluated based on the optimum conditions determined by the manufacturers (Fig. SM1a). The results confirmed the optimal conditions specified by the Manufacturers. The degradation experiments by free enzymes were performed under optimum conditions for each enzyme (Fig. SM1b). Esterase from *Bacillus subtilis* degraded 100% of DBP at 30 °C within 15 min, however, esterase from *Bacillus stearothermophilus* was able to degrade $3.7 \pm 0.9\%$ of DBP at 60 °C at the same time. As for degradation experiments conducted using lipase enzymes for 15 min, whereas Lipozyme CALB and Lipozyme TL 100 degraded $17.6 \pm 1.17\%$ and $35.2 \pm 0.2\%$ of DBP at 50 °C, respectively, Palatase degraded $95.2 \pm 0.7\%$ of DBP at 40 °C.

The esterase from *Bacillus subtilis* exhibited the best result with the highest DBP degradation efficiency (100%) in a short time. According to Eq. (4), the activity of free esterase was determined to be 521.2 U/L at 30 °C. In the literature, there are various studies on the effective use of esterase for the degradation of most PAEs. Saito et al. (2010) investigated the ability of bovine pancreatic cholesterol esterase (CEase) to degrade DBP, DEP, di-n-propyl phthalate (DprP), di-n-pentyl phthalate (DpeP), dihexyl phthalate (DHP), and DEHP. They found that CEase completely degraded all PAEs (5 μ mol) within 15 min. Zhang et al. (2014) investigated the degradation of 10 μ mol PAEs (DEP, DPrP, DBP, DPep, DHP, DEHP, dicyclohexyl phthalate (DCHP), and BBP) using esterase obtained from *Sulfobacillus acidophilus*. They reported that the esterase has a high degradation rate on PAEs with short alkyl side chains, especially DBP. While the esterase was able to degrade 35% to 82% of PAEs (10 mM) within 2 min, it degraded all PAEs within 24 h. Esterase from *Bacillus* sp. K91 was reported to degrade 100% of diisobutyl phthalate (10 mM) over a long duration of time (Ding et al., 2015). Similar to the results of the aforementioned studies, esterase from *Bacillus subtilis* displayed a high ability to degrade DBP in this study. Therefore, this study focused on the immobilization of esterase obtained from *Bacillus subtilis* as the major enzyme responsible for DBP degradation.

3.2. Esterase immobilization

The increase of the enzyme activity and stability and also facilitating the recovery and reuse of the enzyme is a matter of interest and the immobilization of enzymes is a tool commonly applied to fulfill these objectives. In this study, enzyme immobilization was performed by physical adsorption on a nanoclay support (HNTs).

Initially, the enzyme immobilization was studied considering an adsorption time of 360 min, pH 7, E/H 0.02, and temperature of 20 °C, and the results demonstrated that the immobilized enzyme had significant activity and adsorption efficiency. The loading efficiency and specific enzyme activity are different depending on several variables such as pH, adsorption time and temperature, and E/H ratio. Thus, the study of the influence of the selected variables on enzyme adsorption during the immobilization process was then tackled with both composite adsorption efficiency and the activity as the responses (Table SM1).

3.2.1. HNT-enzyme composite adsorption efficiency

The response surface analysis by ANOVA was performed (Table SM2) and the constructed regression model was determined to be significant ($p < 0.05$). Besides, the model F -value was found to be 63.14, and this large F -value related to the p -value showed that the experiment can be modeled with less error (Sadukhan et al., 2016). All the considered variables, the interaction terms between X_1 and X_4 , X_3 and X_4 , and the quadratic terms of the X_1 , and X_4 were significant for the esterase adsorption efficiency. The final model Eq. (7) avoiding the insignificant terms led to a reduction in the equation representing the relationship between the independent variables and the efficiency of enzyme adsorption as follows:

$$Y_1 = 86.06 - 16.11X_1 + 3.45X_2 + 2.17X_3 - 8.70X_4 - 9.27X_1X_4 + 4.75X_3X_4 - 8.39X_1^2 - 21.82X_4^2 \quad (7)$$

Among them, X_2 , and X_3 , an interaction term between X_3 and X_4 exhibited a positive effect on the efficiency of enzyme adsorption. However, X_1 , X_4 , the interaction term between X_1 and X_4 , and the quadratic terms of X_1 and X_4 showed a negative effect on the adsorption efficiency of esterase. To evaluate the quality of curve fitting, the coefficient of determination (R^2) and the adjusted coefficient of determination (Adj- R^2) was found to be 0.98 and 0.96, respectively. These values showed that the model has a high capability to predict the responses. Furthermore, the predicted R^2 (Pred- R^2) of 0.90 was in reasonable agreement with the Adj- R^2 . Adequate Precision (Adeq. Precision) is known to be a test that measures the signal-to-noise ratio (Dritsa et al., 2009). This ratio is used to compare the range of the predicted values at design points to the average of the prediction error. If the ratio is higher than 4, it is considered acceptable. For the adsorption efficiency, it was found to be 28.06. This also can be concluded in the model is significant. The value associated with the Adeq. Precision suggests that obtained model can be used to navigate the design space. The coefficient of variance (C.V.) of 5.29% indicated that the experiment had a very high precision and good reliability. The 3D response surface and 2D contour plots showing the effect of some independent parameters on the enzyme adsorption efficiency are given in Fig. 1.

As can be seen in Figs. 1a and 1b, the maximum adsorption efficiency (95.4%) was obtained when the adsorption time and the E/H ratio were at 360 min and 0.2 mg/mg with temperature and pH considered in the middle points, respectively. The adsorption efficiency improved with the increase in the E/H ratio and the prolonged adsorption time. The adsorption efficiency tends to increase along with the rise in the amount of adsorbent and enzyme (Wang et al., 2015; Mohammadi et al., 2020). Wang et al. (2015) observed a decrease in adsorption efficiency when the E/H ratio was reduced by two-fold. Ilgu et al. (2011) reported that there was almost no change in the immobilization efficiency of the enzyme when the amount of their support material was increased from 1.5 to 3 mg. Similarly, increasing the amount of HNTs did not make a significant difference in the adsorption efficiency in this study. This may be because a low amount of HNTs is sufficient for the adsorption of a low amount of the enzyme. Moreover, a high E/H ratio should be chosen to minimize oversaturated HNTs which can cause inappropriate and non-specific chemical adsorption (Wang et al., 2015).

In Figs. 1c and 1d, the maximum adsorption efficiency was determined at the center points where the temperature was 30 °C and the pH was 6. While the pH value did not have a significant effect on the adsorption efficiency, the temperature had a positive effect on the adsorption efficiency up to a certain temperature and then the efficiency began to decrease with the increase in the temperature. This may be due to the weakening of electrostatic interactions between enzyme and support at high temperatures (You et al., 2015). Twaig et al. (2017) reported that the amount of active sites on the surface of HNTs increases with increasing temperature and adsorption efficiency hereby increases. They observed a decrease in the adsorption capacity over 35 °C and suggested that this decrease may be related to the conformational change on the enzyme surface or distortion of the HNT structure. Based on this information, it may be more appropriate to set the adsorption temperature below 40 °C for enzyme immobilization.

3.2.2. HNT-enzyme composite specific activity

The analysis by ANOVA of the results attained in the design of experiments concerning this response showed that the model is significant (p -value < 0.05 and F value 1254.63) (Table SM3). The specific activity of esterase was significant ($p < 0.05$) and model Eq. (8) with the significant terms was given as follows:

$$Y_2 = 7.27 + 13.79X_1 + 0.45X_2 + 1.74X_4 - 0.50X_1X_3 + 1.19X_1X_4 + 0.55X_2X_4 + 0.25X_3X_4 + 9.16X_1^2 \quad (8)$$

X_1 , X_2 , and X_4 , the interaction terms between X_1 and X_3 , X_1 and X_4 , X_2 and X_4 , X_3 and X_4 , the quadratic term of X_1 played a significantly important role in the specific enzyme activity. The interaction term between X_1 and X_3 displayed a negative effect on the specific enzyme activity. X_1 was the most significant factor affecting the specific enzymatic activity ($F = 14842.97$). Both the R^2 and the Adj- R^2 were found to be 0.99. These results indicated a great connection between the predicted values and the actual values obtained as a result of the experiment. Besides, the Pred- R^2 was determined to

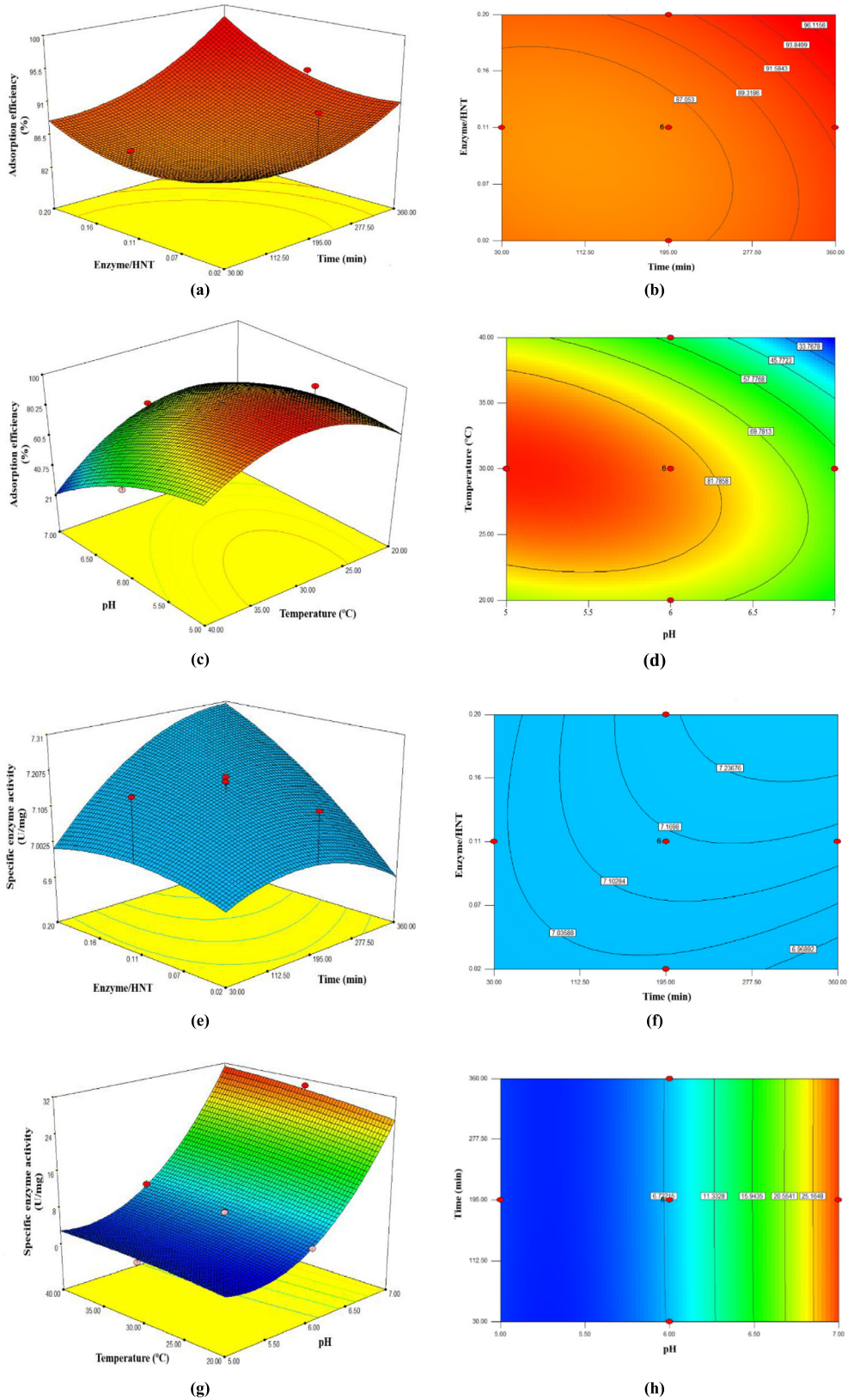


Fig. 1. 3D response surface and 2D contour plots: The effect on adsorption efficiency of (a-b) E/H and time, (c-d) temperature and pH, and the effect on the specific enzyme activity of (e-f) the E/H and time; (g-h) temperature and pH.

be 0.99. It was in reasonable agreement with the value of the Adj- R^2 . The F -value of the model with 1254.63 implied that the model was significant. The Adeq. Precision value was obtained as 90.79. This value indicated the constructed model was usable for navigating the design space. The C.V. (3.80%) which had a very low value, showed a very high degree of precision and good reliability of the experiment. The 3D response surface and 2D contour plots showing the interaction of the model-independent parameters on the specific enzyme activity are given in Fig. 1.

As shown in Figs. 1e and 1f, the highest specific enzyme activity was achieved when the E/H ratio and the adsorption time were 0.2 mg/mg and 360 min, respectively. With a rise in the E/H ratio and adsorption time, the enzyme-specific activity increased. However, the E/H ratio and the adsorption time had no significant effect on the enzyme-specific activity in this study. Wang et al. (2015) reported that the amount of loaded enzyme and enzyme activity increased when the incubation time was prolonged and then they reached an equilibrium. In this study, enzyme activity decreased with the high amount of HNTs (Low E/H) and increased with the high amount of enzyme (high E/H) and then it plateaued. Wang et al. (2010) studied laccase immobilization on silica nanoparticles and reported a similar trend for the laccase enzyme. Mohammadi et al. (2020) investigated the effects of the amount of HNTs and enzyme on specific enzyme activity. They reported that the enzyme activity decreased at a high amount of HNTs and enzyme. Besides, Wang et al. (2015) reported that the amount of adsorbed lipase enzyme and enzyme activity increased with the increase in the enzyme concentration and then reached a plateau. Lee et al. (2009) adsorbed a commercial porcine pancreas lipase on the surface of modified nano-sized magnetite particles and observed that increased lipase concentration had an optimum concentration because more than optimum value caused a decrease in specific enzyme activity due to protein-protein interaction hindrance (Jiang et al., 2009).

As seen in Figs. 1g and 1h, the pH and adsorption temperature at which the enzyme has the highest specific activity were determined to be 7 and 40 °C, respectively. The specific enzyme activity increased when pH and adsorption temperature rose and then reached a plateau in this study. Generally, the temperature has a positive effect on the enzyme activity up to a certain temperature and then the activity begins to decrease as the temperature increases (Osho et al., 2016).

3.2.3. Optimization of the conditions for the enzyme immobilization

Based on the obtained results, the optimization of the variables was carried out considering simultaneously both responses studied. To maximize both responses, Design Expert 8 software was used. The optimum conditions for esterase immobilization were determined to be the pH of 7, the adsorption time of 360 min, the E/H ratio of 0.2 and the adsorption temperature of 30 °C, and the adsorption efficiency and the specific enzyme activity predicted with the model were 73.15% and 29.05 U/mg, respectively, with a desirability value of 0.796. After immobilization, the relative activity of the esterase was determined to be 82.7%. These results were validated experimentally and the attained results were quite similar to the predicted (71.86%, 28.5 U/mg). Under the optimal conditions, the loaded amount of enzyme on HNTs was determined to be 1.922 mg/mg. Ilgu et al. (2011) immobilized the thermophilic recombinant esterase on chitosan nanoparticles. They found the loading amount of the esterase on the nanoparticles as 0.85 mg/mg. Thorn et al. (2011) reported the loading amount of feruloyl esterase on mesoporous silica materials (MPS-5D and MPS-9D) and non-porous silica as 0.034, 0.073, and 0.031 mg/mg, respectively. Bonzom et al. (2018) determined the maximum loading amount of the esterase on MPS to be 0.022 ± 0.03 mg enzyme/mg MPS. Compared to the other studies, the loaded amount of esterase on HNTs in this study (1.922 mg/mg) is noticeable and it can be attributed to the structure of HNTs due to specific sites in and out of the lumen.

3.3. Characterization analysis

Once the optimal conditions were determined, the composite was characterized and its structural and morphological properties were evaluated.

3.3.1. Structural characterization of HNTs and HNT-enzyme composite

The characterization of the composite structure was performed using XRD, SEM, and TEM microscopy (Fig. 2a-d). The observed diffraction peaks are indexed to the hexagonal structure of HNT ($\text{Al}_2\text{Si}_2\text{O}_5(\text{OH})_4$) based on the reported values of Halloysite 7 Å which complies with lattice constants: $a = b = 5.13$, $c = 7.16$ (JCPDS 00-029-1487). Bragg's law (Eq. (9)) is used to determine the d -spacing (the interlayer distance between the layers of HNT).

$$\lambda = 2d \cdot \sin\theta \quad (9)$$

λ is the wavelength of the X-ray sent on the samples, and θ is the diffraction angle.

HNTs showed the first diffraction peak (001) at 12.1° corresponding to a basal spacing of 0.73 nm. A second diffraction peak (100) at 20.1° attributed to 0.44 nm indicates the tubular structure of HNTs. Also, other diffraction peaks at 24.5° (002), 35° (110), 37.9° (003), 54.5° (210), and 62.5° (300) with lower intensity are ascribed to Halloysite 7 Å (Zhai et al., 2013).

The three-dimensional structure of pure HNTs and their surface was studied using SEM. The average length of the HNTs varies between 0.4 and 1 μm and its external diameter ranges from 70 to 100 nm. Additionally, its internal diameter is found to be more or less 30 nm, and its average wall thickness is 10 nm.

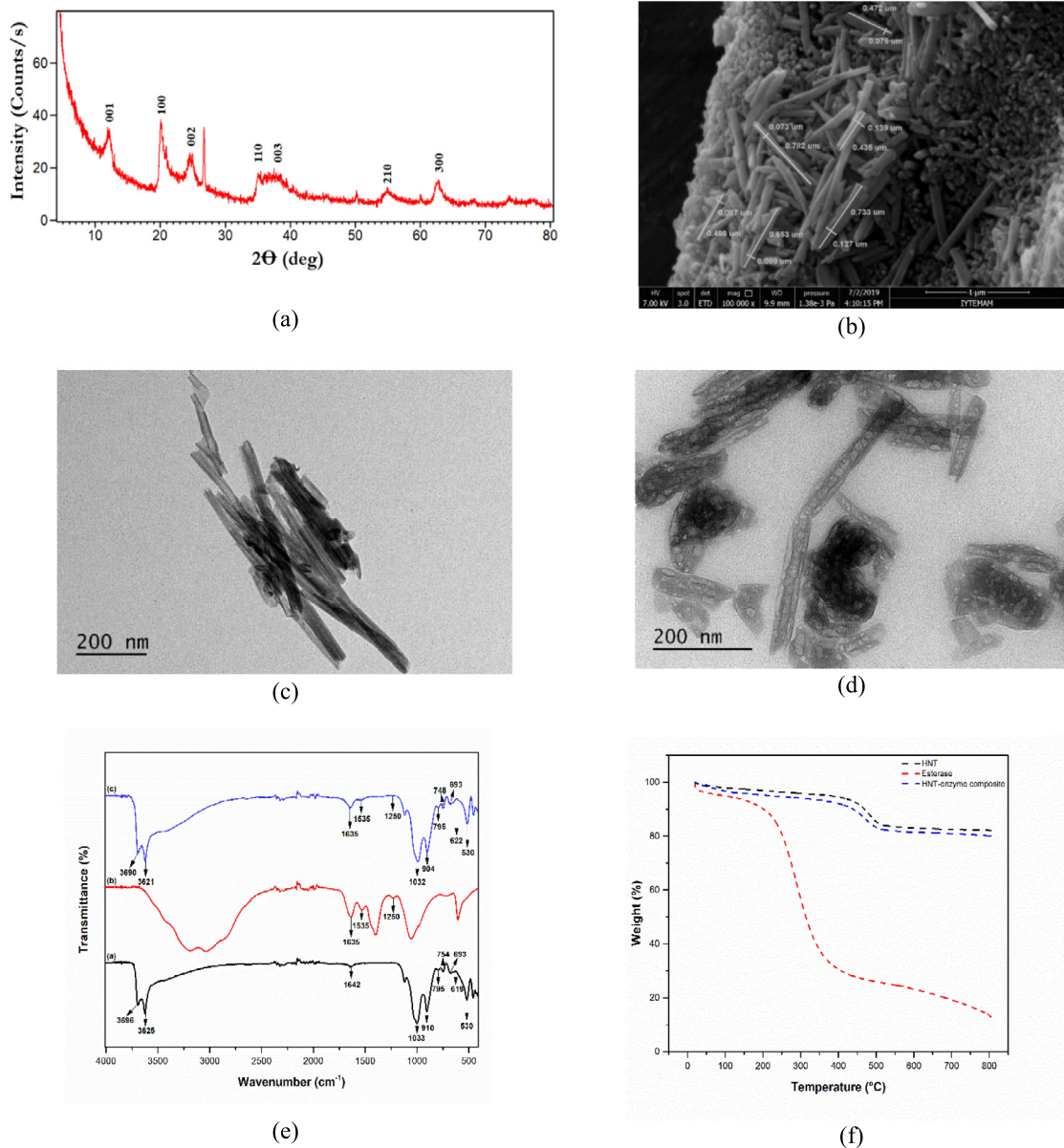


Fig. 2. Composite characterization: XRD analysis (a), SEM images (b), and TEM images of HNTs (c) and HNT-enzyme composite (d), FT-IR spectrum (e) and TGA curves (f) of HNT (black), esterase (red), and HNT-enzyme composite (blue). (For interpretation of the references to color in this figure legend, the reader is referred to the web version of this article)

TEM images of the pure HNTs (Fig. 2c) and HNT-enzyme composite (Fig. 2d) showed that HNTs have a hollow tubular structure, and their two ends are open. Thus, after adsorption, esterase may be immobilized to the lumen and surface of HNTs. After enzyme immobilization, small irregular formations were observed in the lumen and surface of the HNTs, confirming the adsorption of esterase to the HNTs. Similar results are reported in the literature by Tully et al. (2016) who immobilized lipase enzymes to HNTs.

3.3.2. Nanotextural and chemical characterization of HNT-enzyme composite

N_2 adsorption-desorption analysis was performed to determine the adsorption efficiency according to the changes in Brunauer-Emmett-Teller (BET) surface area, pore volume, and pore diameter. BET surface area and pore volume of pure HNTs were calculated to be $66.064 \text{ m}^2/\text{g}$ and $0.002772 \text{ cm}^3/\text{g}$, respectively. When the enzyme is immobilized on the support material, the surface area of HNTs decreases (Rodrigues et al., 2008). When the HNTs showed a decrease in BET surface area from $66.064 \text{ m}^2/\text{g}$ to $37.8918 \text{ m}^2/\text{g}$ (42.64% decrease) after the esterase adsorption, the micropore

volume of HNTs diminished from 0.002772 to 0.001632 cm³/g (41.12% decrease). When the average pore diameter of the HNT-enzyme composite was found to be 107,931 Å, that of HNTs was 90,325 Å. Following the enzyme adsorption, the decrease in the surface area and pore volume and the increase in pore diameter of HNTs could be implications for enzyme immobilization on HNTs.

The structure of the nanotextured composite was investigated by the FT-IR spectrum of HNTs and esterase (Fig. 2e). The infrared spectrum of pure HNT characteristic peaks shows the O-H stretching of water at 3696 cm⁻¹, the OH deformation of water at 3625 cm⁻¹, and in-plane Si-O stretching at 1033 cm⁻¹. In addition, the peaks at 910 cm⁻¹ and 693 cm⁻¹ are caused by deformation vibrations of hydroxyl groups. Lastly, the peaks at 754 cm⁻¹ and 540 cm⁻¹ could be attributed to perpendicular stretching of Si-O and deformation of Al-O-Si, respectively. The amide I (1630 cm⁻¹) and amide II (1535 cm⁻¹) bands are the two most prominent vibrational bands of the protein backbone. It is apparent that both the amide bands and characteristic peaks of HNTs in the spectrum of HNT-enzyme composite are observed. There are significant differences between the peaks of HNTs and HNT-enzyme composite. Several researchers have attempted to immobilize lipase on HNTs. They have obtained similar results demonstrating that the adsorption method is a practicable method for enzyme immobilization on the HNTs (Wang et al., 2015; Mohammadi et al., 2020).

TGA was performed to prove that proteins adsorb onto HNTs (Fig. 2f). It is shown that HNTs have undergone dehydration of the physically adsorbed water at 30 °C and interlayer water molecules bound by hydrogen bonds at 250 °C, and the dehydroxylation process at 470 °C. It is known that the decomposition of protein under air flow shows a maximum mass loss in the range of 300 °C and 350 °C (Duce et al., 2017). In addition, a shoulder forms at 245 °C due to the polypeptide chain thermal decomposition of esterase. At 450 °C and 650 °C, esterase undergoes the decomposition of aggregates as well as the carbonizing and ashing of the hard residues of the proteins (Duce et al., 2017). Compared to the HNT-enzyme composite, the free esterase displayed rapid decomposition with the increasing temperature due to enzyme denaturation. The pure HNTs and the free esterase displayed a mass loss of 17.53% and 87.27%, respectively in the range of 20 °C and 800 °C. As for the HNT-enzyme composite, the weight loss percentage was determined to be 20.05% within the same temperature range. These results exhibited that the enzyme adsorption on HNTs significantly improved the thermal resistance of the enzyme.

3.4. Stability tests

3.4.1. Thermal stability

With the increase in temperature, the HNT-enzyme composite showed a 17.5% loss in activity at 70 °C while the free esterase enzyme only maintained about 5.7% of its original activity at the same temperature (Fig. SM2a). The enzyme immobilization resulted in enhanced thermal stability at higher temperatures, which is attributed to an increase in rigidity achieved during the immobilization process. This rigidity helps to prevent conformational changes in the enzyme's tertiary structure (Hartmeier, 1988; Zhai et al., 2010). Consequently, immobilized enzymes have the potential to be used in a wide range of industrial applications (Hu et al., 2007).

3.4.2. Storage stability

As shown in Fig. SM2b, at the end of storage time for 14 days, the free esterase lost almost 21% of its original activity, whereas the HNT-enzyme composite still retained 92% of its initial activity. Zhai et al. (2010) reported that the immobilized urease and α -amylase on HNT retained 90% and 94% of their initial activities, respectively after 15 days of storage time. Wang et al. (2015) conducted a test to evaluate the stability of immobilized lipase on HNTs. They reported that the immobilized lipase maintained more than 80% of the initial activity at the end of 14 days storage, while free lipase lost almost all of the original activity at the same time. This fact indicates that HNTs can offer a conducive environment for immobilized enzymes, resulting in significantly improved storage stability.

3.4.3. Reusability of HNT-enzyme composite

Enzymes that have been immobilized on supports can be readily recovered and reused multiple times, which is not possible with free enzymes that are difficult to separate from the reaction mixture. In the literature, the relative enzyme activities after 7 repeated use following the immobilization of α -amylase (Zhai et al., 2010), urease (Zhai et al., 2010), and lipase (Mohammadi et al., 2020) onto HNTs were reported as 56.2%, 65%, and 70%, respectively. In this study, the HNT-enzyme composite exhibited significant stable activity even after 7 continuous cycles of the enzymatic reaction and it retained almost 75% of its initial activity (Fig. SM3). This result demonstrated much better reusability of HNT-esterase composite compared to other immobilized enzymes on HNTs. This may be attributed to biocompatibility between enzyme and HNTs. Additionally, the loss in activity can be due to enzyme inactivation resulting from its repeated use (Zhai et al., 2010).

3.5. Determination of kinetic parameters

The K_m and V_{max} of free esterase and HNT-esterase composite were determined using the Lineweaver–Burk plots (data not shown). The Lineweaver–Burk plots demonstrated a linear relationship within the tested concentration range. When the K_m and V_{max} of free esterase were 0.673 μ M and 35.461 μ M/min, respectively, these values of the HNT-enzyme

composite were determined to be 1.76 μM and 52.6 $\mu\text{M}/\text{min}$, respectively. The K_m value for the HNT-esterase composite was found to be higher than that of the free esterase, indicating that the HNT-enzyme composite had a lower affinity for the substrate and a lower tendency to interact with it. Similar results were reported in the literature (Pereira et al., 2019; Mohammadi et al., 2020) which the HNT-enzyme composite exhibited a higher K_m value than free esterase. Furthermore, the V_{max} value of the HNT-enzyme composite was 1.5-fold higher than that of the free esterase. The immobilization process can lead to changes in the structure of the enzyme and alter its accessibility to the substrate, which can affect the kinetic parameters. Therefore, differences in the K_m and V_{max} values between the free and immobilized enzymes can be attributed to these changes (Akgöl et al., 2001; Tutar et al., 2009). In addition, the increase in the V_{max} value of the HNT-enzyme composite, despite the increase in the K_m value, may be attributed to a decrease in enzyme inhibition (Rodrigues et al., 2013). The K_m and V_{max} values obtained in this study may be lower than those obtained in the literature (Tekedar and Sanli-Mohamed, 2011; Mohammadi et al., 2020). The enzyme with low K_m and V_{max} indicates better enzyme-substrate binding (Sudo, 1995; Saganuwan, 2021). This fact shows that the esterase enzyme used in the study has a high affinity with its substrate.

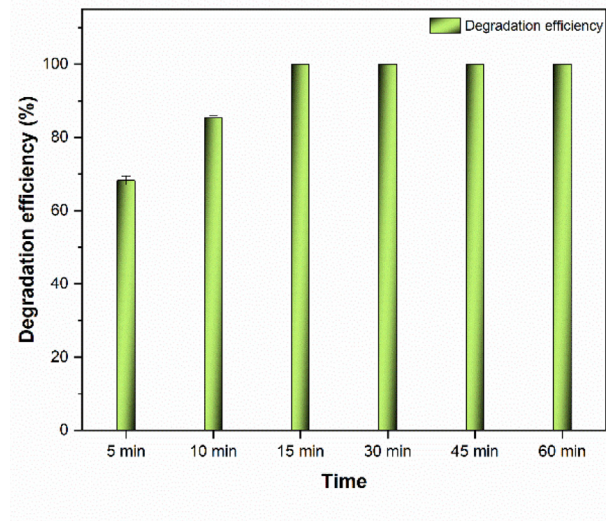
3.6. DBP degradation study by HNT-enzyme composite

The results of the degradation experiment showed that the free esterase enzyme (1 mg/mL) completely degraded DBP (100 mg/L) within 15 min (Fig. 3a), and the HNT-enzyme composite continued the degradation of DBP until the end of the 3rd cycle with a 100% efficiency (Fig. 3b). Moreover, the HNT-enzyme composite was able to degrade almost 70% of 100 mg/L DBP at the end of the 7th cycle. It can be used in long cycles for DBP degradation although the free esterase could not be used repeatedly due to the need to separate from the reaction mixture. This may be because only a part of the HNT-enzyme composite comes into contact with DBP. Therefore, the HNT-enzyme composite exhibits good degradation capability even after repeated use. In recent years, a few studies have focused on the degradation of DBP in the presence of an enzyme immobilized on various materials. Dulazi and Liu (2011) immobilized lipase enzyme on chitosan beads to degrade different types of PAEs (15 mg/L). They reported that the lipase immobilized on chitosan beads degraded 73.05% of DBP in a solution consisting of a mixture of different types of PAEs. Sungkeeree et al. (2017) conducted a DBP degradation study using an immobilized esterase obtained from *Sphingobium* sp. SM42 on amine-functionalized supports. They reported that the immobilized esterase degraded 99% of 10 mM DBP and 30% of 100 mM DBP within 18 h. In this study, the HNT-enzyme composite with high activity exhibited high degradation efficiency in long cycles. It may be related to the biocompatibility between the esterase and HNTs. Because the reusability of the immobilized enzyme depends on the support material and the substrate (Zhai et al., 2010).

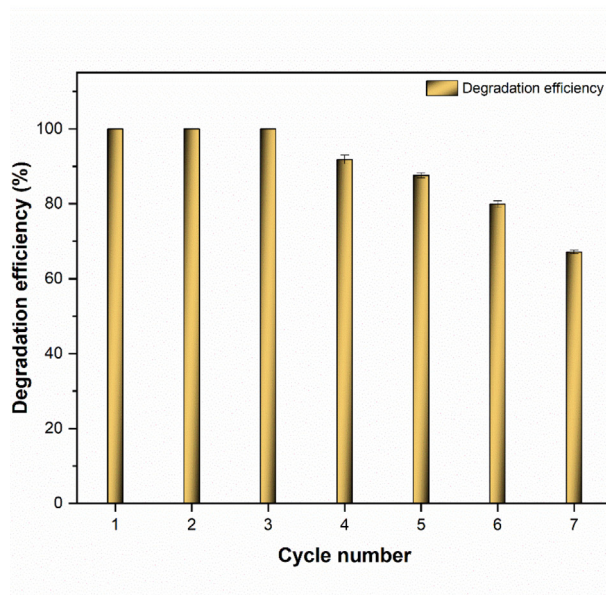
Contrary to the free esterase, the HNT-enzyme composite could be separated easily in the reaction mixture and subsequently reused. At the end of each degradation cycle, the activity of the composite was assayed again. Free esterase enzyme could not be reused in degradation experiments. During the degradation experiments with the 7 cycles of 1h-periods, the relative activity and the mass percentage of the esterase immobilized on HNTs were given (data not shown). The mass percent of the esterase on HNTs was 71% at the 3rd cycle and this percentage was determined to be 48% at the end of the experiment. It was understood that approximately 50% of the esterase immobilized on HNTs was released at the end of the experiment. Furthermore, while the esterase immobilized on HNTs retained 70% of its initial activity in the 3rd cycle in the degradation experiment, it lost 55% of initial activity at the end of the 7th cycle. This decrease in the activity of the HNT-enzyme composite can be attributed to the accumulation of metabolites that covers the enzyme and has an effect on the next degradation cycles (Zhai et al., 2013).

3.7. Investigation of DBP metabolites

After the degradation experiments, the metabolites of DBP were identified based on mass spectra at a particular retention time (RT) as shown in Fig. SM4. DBP solution without the esterase was used as the control sample in HPLC-MS analysis (Fig. SM4a). The obtained m/z ratios by mass spectrometry were compared to those of compounds in the literature. The m/z ratio for DBP was 279.15 (RT 22.6 min). After degradation experiments in the presence of free esterase, phthalic anhydride (M1; m/z 149.02; RT 2.8 min), DMP (M2; m/z 163.0388; RT 6.9 min), mono butyl phthalate (MBP; M3; m/z 223.0961; RT 9.7 min) and butyl methyl phthalate (BMP; M4; m/z 259.039; RT 15.4 min) were detected as the metabolites of DBP (m/z) in the presence of methanol (Fig. SM4b). MBP, BMP, and DMP are likely to be formed by transesterification reaction in the presence of methanol as a result of the DBP degradation experiments (Kim and Lee, 2005; Ahn et al., 2006; Kumar et al., 2017). Besides, Okamoto et al. (2011) reported that PAEs undergo transesterification which is the process of exchanging the alkyl group of an ester with the alkyl group of an alcohol. Phthalic acid (PA) which is formed by the de-esterification reaction of PMEs was reported in many studies as a metabolite of PAEs via bacterial (Feng et al., 2002) or enzymatic degradation (Saito et al., 2010; Dulazi and Liu, 2011). Then, phthalic anhydride is formed as a result of the dehydration of PA. In this study, the other peaks observed in the chromatograms were determined to be polymer. Kim and Lee (2005) studied the degradation of DBP by free esterase and cutinase. They identified three metabolites; 1,3 isobenzofurandione (IBF), DMP, and BMP. In the study, firstly, DBP was converted to 1,3 isobenzofurandione (IBF) at the end of 7.5 h in the presence of cutinase and then, the amount of BMP began to increase as that of IBF decreased after the 3rd day. It was reported that BMP was the major metabolite of DBP degradation conducted



(a)



(b)

Fig. 3. DBP degradation efficiency in the presence of (a) free esterase and (b) HNT-enzyme composite.

using the esterase. IBF was not detected in this study. This is because the formation of the metabolites significantly depends on the enzyme used in the study. IBF is a major degradation product in the DBP degradation study in the presence of cutinase (Ahn et al., 2006). Fang et al. (2010) conducted a study on DBP degradation using a bacteria (*Enterobacter* sp. T5) isolated from municipal solid waste and they reported that the major DBP metabolites were MBP and PA. Kumar et al. (2017) conducted a study on the biodegradation of DBP using two isolated bacteria (*Pseudomonas* sp. V21b and *Comamonas* sp. 51F) from municipal solid waste. They identified MBP and PA to be the metabolites of DBP. Fang et al. (2017) investigated the biodegradation of DBP in the presence of *Acinetobacter* sp. strain LMB-5 isolated from soil. There were four metabolites of DBP, 1,2 benzenedicarboxylic acid, butyl methyl ester, DMP, and PA during DBP degradation. Generally, most DBP metabolites identified in the literature were found as a result of DBP degradation in the presence of the esterase in this study. It is apparent from Fig. SM4c that MBP, BMP, DMP, and phthalic anhydride appeared in

the HPLC chromatogram at the end of the degradation experiment conducted using the HNT-enzyme composite for 1 h. PAEs and their metabolites tend to be adsorbed in the support materials (Dulazi and Liu, 2011). Compared to Fig. SM4b and SM4c, there were differences in the peak areas of metabolites that occurred in the presence of free enzyme and HNT-enzyme composites. This fact may be due to the adsorption of some PAE metabolites on the HNT-enzyme composite. For this reason, the peak area may be visible at a lower intensity. As seen in the HPLC-MS chromatograms, all metabolites that appeared in the presence of free esterase during DBP degradation were found in the presence of the HNT-enzyme composite. As a result of this study, it is understood that the HNT-enzyme composite metabolizes DBP to phthalic anhydride. This may be an indication that the esterase does not lose its characteristic properties after immobilization and can be used as an effective degrader during long cycles of degradation experiments.

4. Conclusion

In this study, the ability of esterase and lipase enzymes obtained from various microorganisms to degrade DBP was investigated. Esterase from *Bacillus subtilis* displayed the highest DBP degradation ability and then it was immobilized on halloysite nanotubes (HNTs) with the adsorption method under optimal conditions. The HNT-enzyme composite was repeatedly used in the DBP degradation over time, retaining most of its initial activity. Whereas the free esterase revealed a high ability to degrade DBP in a short time, the immobilized esterase could be used with a high degradation ability during long cycles. It has been confirmed that HNTs are a desirable natural support material to overcome the limitation of enzyme catalytic activity, and also the esterase obtained from *Bacillus subtilis* is an effective degrader of DBP. All these results support the fact that the HNT-enzyme composite can be more suitable for future practical applications in the remediation of phthalic acid esters in different environments.

CRedit authorship contribution statement

Esin Balci: Investigation, Writing – original draft, Methodology, Formal analysis, Data curation. **Emilio Rosales:** Investigation, Methodology, Validation, Formal analysis, Writing – review & editing. **Marta Pazos:** Funding acquisition, Supervision, Writing – review & editing. **Aysun Sofuoglu:** Writing – review & editing. **Maria Angeles Sanromán:** Supervision, Funding acquisition, Project administration, Conceptualization, Writing – review & editing.

Declaration of competing interest

The authors declare that they have no known competing financial interests or personal relationships that could have appeared to influence the work reported in this paper.

Data availability

Data will be made available on request.

Acknowledgments

This research was funded through the 2019–2020 Biodiversa & Water JPI joint call for research proposals, under the BiodivRestore ERA-Net COFUND programme. Project PCI2022-132941 was funded by MCIN/AEI/10.13039/501100011033 and European Union NextGeneration EU/PRTR and Xunta de Galicia and ERDF (ED431C 2021-43). Additionally, the research has been provided with financial support by the Scientific and Technological Research Council of Turkey (TUBITAK) under the 2214-A Doctoral Research Fellowship Program. Funding for open access charge: Universidade de Vigo/CISUG.

Appendix A. Supplementary data

Supplementary material related to this article can be found online at <https://doi.org/10.1016/j.eti.2023.103113>.

References

- Abdullayev, E., Price, R., Shchukin, D., Lvov, Y., 2009. Halloysite tubes as nanocontainers for anticorrosion coating with benzotriazole. *ACS Appl. Mater. Interfaces* 1 (7), 1437–1443. <http://dx.doi.org/10.1021/am9002028>.
- Ahn, Y.J., Kim, Y.H., Min, J., Lee, J., 2006. Accelerated degradation of dipentyl phthalate by *Fusarium oxysporum* f. sp. *pisi* cutinase and toxicity evaluation of its degradation products using bioluminescent bacteria. *Curr. Microbiol.* 52 (5), 340–344. <http://dx.doi.org/10.1007/s00284-005-0124-9>.
- Akgöl, S., Kacar, Y., Denizli, A., Arica, M., 2001. Hydrolysis of sucrose by invertase immobilized onto novel magnetic polyvinylalcohol microspheres. *Food Chem.* 74 (3), 281–288. [http://dx.doi.org/10.1016/S0308-8146\(01\)00150-9](http://dx.doi.org/10.1016/S0308-8146(01)00150-9).
- Balci, E., Rosales, E., Pazos, M., Sofuoglu, A., Sanroman, M.A., 2022. Continuously treatment of diethyl hexyl and dibutyl phthalates by fixed-bed reactor: Comparison of two esterase bionanocomposites. *Bioresour. Technol.* 363, 127990. <http://dx.doi.org/10.1016/j.biortech.2022.127990>.
- Baloyi, N.D., Tekere, M., Maphangwa, K.W., Masindi, V., 2021. Insights into the prevalence and impacts of phthalate esters in aquatic ecosystems. *Front. Environ. Sci.* 9, 684190. <http://dx.doi.org/10.3389/fenvs.2021.684190>.

- Bilal, M., Rashid, E.U., Zdzarta, J., dos Santos, J.C.S., Fernandes, P.C.B., Cheng, H., Jesionowski, T., 2022. Engineering magnetic nanobiocatalytic systems with multipurpose functionalities for biocatalysis, biotechnology and bioprocess applications. *Sustain. Chem. Pharm.* 30, 100866. <http://dx.doi.org/10.1016/j.scp.2022.100866>.
- Bonzom, C., Schild, L., Gustafsson, H., Olsson, L., 2018. Feruloyl esterase immobilization in mesoporous silica particles and characterization in hydrolysis and transesterification. *BMC Biochemistry* 19 (1), 1–12. <http://dx.doi.org/10.1186/s12858-018-0091-y>.
- Bradford, M.M., 1976. A rapid and sensitive method for the quantitation of microgram quantities of protein utilizing the principle of protein-dye binding. *Anal. Biochem.* 72 (1–2), 248–254. [http://dx.doi.org/10.1016/0003-2697\(76\)90527-3](http://dx.doi.org/10.1016/0003-2697(76)90527-3).
- Brena, B., González-Pombo, P., Batista-Viera, F., 2013. Immobilization of enzymes: A literature survey. *Immobil. Enzym. Cells* 1051, 15–31. http://dx.doi.org/10.1007/978-1-62703-550-7_2.
- Cao, J., Mo, J., Sun, Z., Zhang, Y., 2018. Indoor particle age. A new concept for improving the accuracy of estimating indoor airborne SVOC concentrations, and applications. *Build. Environ.* 136, 88–97. <http://dx.doi.org/10.1016/j.buildenv.2018.03.028>.
- Cavalcante, F.C.T.T., Falcao, I.R.A., Souza, J.E.S., Rocha, T.G., de Sousa, I.G., Cavalcante, A.L.G., de Oliveira, A.L.B., dos Santos, J.C.S., 2021. Designing of nanomaterials-based enzymatic biosensors: Synthesis, properties, and applications. *Electrochemistry* 2 (1), 149–184. <http://dx.doi.org/10.3390/electrochem2010012>.
- Cruz-Ortiz, B.R., Rios-Gonzalez, L.J., Garza Garcia, Y., Rodrigues de la Garza, J.A., Rodrigues-Martinez, J., 2011. Immobilization of *Thermomyces lanuginosus* lipase in PVA-alginate beads. *J. the Mexican Chemical Society* 55 (3), 176–188. <http://dx.doi.org/10.29356/jmcs.v55i3.817>.
- Ding, J., Wang, C., Xie, Z., Li, J., Yang, Y., Mu, Y., Tang, X., Xu, B., Zhou, J., Huang, Z., 2015. Properties of a newly identified esterase from *Bacillus* sp. K91 and its novel function in diisobutyl phthalate degradation. *PLoS One* 10 (3), e0119216. <http://dx.doi.org/10.1371/journal.pone.0119216>.
- Dritsa, V., Rigas, F., Doulia, D., Avramides, E.J., Hatzianestis, I., 2009. Optimization of culture conditions for the biodegradation of lindane by the polypore fungus *Ganoderma Australe*. *Water Air Soil Pollut.* 204, 19–27. <http://dx.doi.org/10.1007/s11270-009-0022-z>.
- Duce, C., Porta, V.D., Bramanti, E., Campanella, B., Spepi, A., Tine, M.R., 2017. Loading of halloysite nanotubes with BSA, α -Lac, and β -Lg: A fourier transform infrared spectroscopic and thermogravimetric study. *Nanotechnology* 28, <http://dx.doi.org/10.1088/1361-6528/28/5/055706>.
- Dulazi, A.A., Liu, H., 2011. Removal of phthalate esters from water using immobilized lipase on chitosan beads. *Environ. Technol.* 32 (13), 1443–1451. <http://dx.doi.org/10.1080/09593330.2010.538932>.
- Fang, C.R., Yao, J., Zheng, Y.G., Jiang, C.J., Hu, L.F., Wu, Y.Y., Shen, D.S., 2010. Dibutyl phthalate degradation by *Enterobacter* sp. T5 isolated from municipal solid waste in landfill bioreactor. *Int. Biodeterioration Biodegrad.* 64 (6), 442–446. <http://dx.doi.org/10.1016/j.ibiod.2010.04.010>.
- Fang, Y., Zhang, L., Wang, J., Zhou, Y., Ye, B., 2017. Biodegradation of phthalate esters by a newly isolated *Acinetobacter* sp. Strain LMB-5 and characteristics of its esterase. *Pedosphere* 27 (3), 606–665. [http://dx.doi.org/10.1016/S1002-0160\(17\)60355-2](http://dx.doi.org/10.1016/S1002-0160(17)60355-2).
- Feng, Z., Kunyan, C., Jiamo, F., Guoying, S., Huifang, Y., 2002. Biodegradability of di (2-ethylhexyl) phthalate by *Pseudomonas fluorescens* FS1. *Water Air Soil Pollut.* 140 (1), 297–305. <http://dx.doi.org/10.1023/A:1020108502776>.
- Ferrari, P.C., Araujo, F.F., Pianaro, S.A., 2017. Halloysite nanotubes-polymeric nanocomposites: characteristics, modifications, and controlled drug delivery approaches. *Ceramica* 63, 423–431. <http://dx.doi.org/10.1590/0366-69132017633682167>.
- Gass, S.E., Sandoval, M.L., Talou, M.H., Martinez, A.G.T., Camerucci, M.A., Gregorova, E., Pabst, W., 2015. High temperature mechanical behavior of porous cordierite based ceramic materials evaluated using 3-point bending. *Procedia Mater. Sci.* 9, 254–261. <http://dx.doi.org/10.1016/j.mspro.2015.04.032>.
- Hartmeier, W., 1988. *Immobilized Biocatalysts-An Introduction*. Springer-Verlag, New York.
- He, H., Zhang, S., Liu, X., 2015. Immobilization of feruloyl esterases on magnetic nanoparticles and its potential in production of ferulic acid. *J. Biosci. Bioeng.* 120 (3), 330–334. <http://dx.doi.org/10.1016/j.jbiosc.2015.01.006>.
- Hu, X., Zhao, X., Hwang, H.M., 2007. Comparative study of immobilized *Trametes versicolor* laccase on nanoparticles and kaolinite. *Chemosphere* 66 (9), 1618–1626. <http://dx.doi.org/10.1016/j.chemosphere.2006.08.004>.
- Huang, L., Zhu, X., Zhou, S., Cheng, Z., Shi, K., Zhang, C., Shao, H., 2021. Phthalic acid esters: Natural sources and biological activities. *Toxins* 13 (7), 495. <http://dx.doi.org/10.3390/toxins13070495>.
- Ilgü, H., Turan, T., Sanlı-Mohammed, G., 2011. Preparation, characterization, and optimization of chitosan nanoparticles as carrier for immobilization of thermophilic recombinant esterase. *J. Macromol. Sci. A Pure Appl. Chem.* 48 (9), 713–721. <http://dx.doi.org/10.1080/10601325.2011.596050>.
- Jiang, Y., Guo, C., Xia, H., Mahmood, I., Liu, C., Liu, H., 2009. Magnetic nanoparticles supported ionic liquids for lipase immobilization: enzyme activity in catalyzing esterification. *J. Mol. Catal. B-Enzymatic* 58, 103–109. <http://dx.doi.org/10.1016/j.molcatb.2008.12.001>.
- Kamble, R., Ghag, M., Gaikawad, S., Panda, B.K., 2012. Halloysite nanotubes and applications: A review. *J. Adv. Sci. Res.* 3 (2), 25–29.
- Kim, Y.H., Lee, J., 2005. Enzymatic degradation of dibutyl phthalate and toxicity of its degradation products. *Biotechnol. Lett.* 27 (9), 635–639. <http://dx.doi.org/10.1007/s10529-005-3631-7>.
- Kong, X., Jin, D., Jin, S., Wang, Z., Yin, H., Xu, M., Deng, Y., 2018. Responses of bacterial community to dibutyl phthalate pollution in a soil-vegetable ecosystems. *J. Hard Mater.* 352, 142–150. <http://dx.doi.org/10.1016/j.jhazmat.2018.04.015>.
- Kumar, V., Sharma, N., Maitra, S.S., 2017. Comparative study on the degradation of dibutyl phthalate by two newly isolated *Pseudomonas* sp. V216 and *Comamonas* sp. 51F. *Biotechnol. Rep.* 15, 1–10. <http://dx.doi.org/10.1016/j.btre.2017.04.002>.
- Lee, D.G., Ponvel, K.M., Kim, M., Hwang, S., Ahn, I.S., Lee, C.H., 2009. Immobilization of lipase on hydrophobic nano-sized magnetite particles. *J. Mol. Catal. B-Enzymatic* 57 (1–4), 62–66. <http://dx.doi.org/10.1016/j.molcatb.2008.06.017>.
- Mohammadi, N.S., Khiabani, M.S., Ghanbarzadeh, B., Mokarram, R.R., 2020. Enhancement of biochemical aspects of lipase adsorbed on halloysite nanotubes and entrapped in polyvinyl alcohol/alginate hydrogel strategies to reuse the most stable lipase. *World J. Microbiol. Biotechnol.* 36 (3), 1–15. <http://dx.doi.org/10.1007/s11274-020-02817-2>.
- Monteiro, R.R.C., Neto, D.M.A., Fecine, P.B.A., Lopes, A.A.S., Gonçalves, L.R.B., dos Santos, J.C.S., de Souza, M.C.M., Fernandez-Lafuente, R.F., 2019. Ethyl butyrate synthesis catalyzed by lipases A and B from *Candida Antarctica* immobilized onto magnetic nanoparticles, improvement of biocatalysts's performance under ultrasonic irradiation. *Int. J. Mol. Sci.* 20 (22), 5807. <http://dx.doi.org/10.3390/ijms20225807>.
- Moreira, K.S., Junior, L.S.M., Monteiro, R.R.C., de Oliveira, A.L.B., Valle, C.P., Freire, T.M., Fecine, P.B.A., de Souza, M.C.M., Fernandez-Lorente, G., Guisan, J.M., dos Santos, J.C.S., 2020. Optimization of the production of enzymatic biodiesel from residual babassu oil (*Orbignya* sp.) via RSM. *Catalysts* 10 (4), 414. <http://dx.doi.org/10.3390/catal10040414>.
- Okamoto, Y., Toda, C., Ueda, K., Hashizume, K., Kojima, N., 2011. Transesterification in microbial degradation of phthalate esters. *J. Health Sci.* 57 (3), 293–299. <http://dx.doi.org/10.1248/jhs.57.293>.
- Osho, M.B., Popoola, T., Adeleye, T.M., Adetunji, M.C., 2016. Response surface methodology for optimal immobilization of *Aspergillus niger* ATCC 1015 lipase by adsorption method. *Int. J. Biol. Res.* 4 (1), 56–63. <http://dx.doi.org/10.14419/ijbr.v4i1.6008>.
- Patel, S., Jammalamadaka, U., Sun, L., Tappa, K., Mills, D.K., 2016. Sustained release of antibacterial agents from doped halloysite nanotubes. *Bioengineering* 3 (1), 1. <http://dx.doi.org/10.3390/bioengineering3010001>.
- Pereira, A.D.S., Diniz, M.M., De Jong, G., Gama Filho, H.S., dos Anjos, M.J., Finotelli, P.V., Fontes-Sant'Ana, G.C., Amaral, P.F., 2019. Chitosan-alginate beads as encapsulating agents for *Yarrowia lipolytica* lipase: Morphological physico-chemical and kinetic characteristics. *Int. J. Biol. Macromol.* 139, 621–630. <http://dx.doi.org/10.1016/j.ijbiomac.2019.08.009>.
- Pirsaheb, M., Zinatizadeh, A.A., 2009. Kinetic evaluation and process performance of a fixed film bioreactor removing phthalic acid and dimethyl phthalate. *J. Hard Mater.* 167, 500–506. <http://dx.doi.org/10.1016/j.jhazmat.2009.0.003>.

- Rao, K.M., Kumar, A., Suneetha, M., Han, S.S., 2018. pH and near-infrared active; chitosan-coated halloysite nanotubes loaded with curcumin-Au hybrid nanoparticles for cancer drug delivery. *Int. J. Biol. Macromol.* 112, 119–125. <http://dx.doi.org/10.1016/j.ijbiomac.2018.01.163>.
- Rodrigues, D.S., Cavalcante, G.P., Ferreira, A.L.O., Goncalves, L.R.B., 2008. Immobilization of *Candida antarctica* lipase type B by adsorption on activated carbon. *Chem. Biochem. Eng. Q.* 22 (1), 125–133.
- Rodrigues, R.C., Ortiz, C., Berenguer-Murcia, A., Torres, R., Fernandez-Lafuente, R., 2013. Modifying enzyme activity and selectivity by immobilization selectivity by immobilization. *Chem. Soc. Rev.* 42, 6290–6307. <http://dx.doi.org/10.1039/C2CS35231A>.
- Rosales, E., Sanromán, M.A., Pazos, M., 2012. Application of central composite face-centered design and response surface methodology for the optimization of electro-Fenton decolorization of Azure B dye. *Environ. Sci. Pollut. Res.* 19, 1738–1746. <http://dx.doi.org/10.1007/s11356-011-0668-0>.
- Sadukhan, B., Mondal, N.K., Chatteraj, S., 2016. Optimisation using central composite design (CCD) and the desirability function for sorption of methylene blue from aqueous solution onto *Lemna major*. *Karbala Int. J. Mod. Sci.* 2 (3), 145–155. <http://dx.doi.org/10.1016/j.kijoms.2016.03.005>.
- Saganuwan, S.A., 2021. Application of modified Michaelis–Menten equations for determination of enzyme inducing and inhibiting drugs. *BMC Pharmacol. Toxicol.* 22 (57), 1–15.
- Saito, T., Tanabe, R., Nagai, K., Kato, K., 2010. Enzymatic hydrolysis of structurally diverse phthalic acid esters by porcine and bovine pancreatic cholesteral esterases. *Chemosphere* 81, 1544–1548. <http://dx.doi.org/10.1016/j.chemosphere.2010.08.020>.
- Sassolas, A., Blum, L.J., Leca-Bouvier, B.D., 2012. Immobilization strategies to develop enzymatic biosensors. *Biotecnol. Adv.* 30 (3), 489–511. <http://dx.doi.org/10.1016/j.biotechadv.2011.09.003>.
- Scholz, N., Diefenbach, R., Rademacher, I., Linneman, D., 1997. Biodegradation of DEHP, DBP, and DNP: Poorly water soluble and widely used phthalate plasticizers. *Bull. Environ. Contam. Toxicol.* 58, 527–534. <http://dx.doi.org/10.1007/s001289900367>.
- Seyoum, A., Pradhan, A., 2019. Effect of phthalates on development, reproduction, fat metabolism and Lifespan in *Daphnia Magna*. *Sci. Total Environ.* 654, 969–977. <http://dx.doi.org/10.1016/j.scitotenv.2018.11.158>.
- Sharma, D., Bhardwaj, K.K., Gupta, R., 2021. Immobilization and applications of esterases. *Biocatal. Biotransform.* 1–16. <http://dx.doi.org/10.1080/10242422.2021.2013825>.
- Sharma, A., Sharma, T., Sharma, T., Sharma, S., Kanwar, S.S., 2019. Role of microbial hydrolases in bioremediation. In: Kumar, A., Sharma, S. (Eds.), *Microbes and Enzymes in Soil Health and Bioremediation*. Springer, Singapore, pp. 149–164. http://dx.doi.org/10.1007/978-981-13-9117-0_7.
- Souza, J.E.S., de Oliveira, G.P., Alexandre, J.Y.N.H., Neto, J.G.L., Sales, M.G., Junior, P.G.S., de Oliveira, A.L.B., de Souza, M.C.M., dos Santos, J.C.S., 2022. A comprehensive review on the use of metal–organic frameworks (MOFs) coupled with enzymes as biosensors. *Electrochemistry* 3 (1), 89–113. <http://dx.doi.org/10.3390/electrochem3010006>.
- Sudo, K., 1995. Enzyme kinetics for enzyme immunoassay. *Nihon Rinsho. Japanese J. Clin. Med.* 53 (9), 2134–2139.
- Sungkeeree, P., Whangsuk, W., Sallabhan, R., Dubbs, J., Mongkolsuk, S., Loprasert, S., 2017. Efficient removal of toxic phthalate by immobilized serine-type aldehyde tagged esterase G. *Process Biochem.* 63, 60–65. <http://dx.doi.org/10.1016/j.procbio.2017.09.009>.
- Tanaka, T., Yamada, K., Tonosaki, T., Konishi, T., Goto, H., Taniguchi, M., 2000. Enzymatic degradation of alkylphenols, bisphenol A, synthetic estrogen and phthalic ester. *Water Sci. Technol.* 42, 89–95. <http://dx.doi.org/10.2166/wst.2000.0556>.
- Tari, G., Bobos, I., Gomes, C.S.F., Ferreira, J.M.F., 1999. Modification of surface charge properties during kaolinite to halloysite-7 Å transformation. *J. Colloid Interface Sci.* 210 (2), 360–366. <http://dx.doi.org/10.1006/jcis.1998.5917>.
- Tekedar, H.C., Sanli-Mohamed, G., 2011. Molecular cloning, over expression, and characterization of thermoalkalophilic esterases isolated from *Geobacillus* sp. *Extremophiles* 15, 203–211. <http://dx.doi.org/10.1007/s00792-010-0344-1>.
- Thorn, C., Gustafsson, H., Olsson, L., 2011. Immobilization of feruloyl esterases in mesoporous materials leads to improved transesterification yield. *J. Mol. Catal. B-Enzymatic* 72 (1), 57–64. <http://dx.doi.org/10.1016/j.molcatb.2011.05.002>.
- Tully, J., Yendluri, R., Lvov, Y., 2016. Halloysite clay nanotubes for enzyme immobilization. *Biomacromolecules* 17 (2), 615–621. <http://dx.doi.org/10.1021/acs.biomac.5b01542>.
- Tutar, H., Yilmaz, E., Pehlivan, E., Yilmaz, M., 2009. Immobilization of *Candida rugose* lipase on sporopollenin from *Lycopodium clavatum*. *Int. J. Biol. Macromol.* 45 (3), 315–320. <http://dx.doi.org/10.1016/j.ijbiomac.2009.06.014>.
- Twaig, F., Chang, K.X., Ling, J.Y.W., 2017. Adsorption of diastase over natural halloysite nanotubes (HNTs). *IOP Conf. Ser. Mater. Sci. Eng.* 206.
- Wang, F., Guo, C., Yang, L.R., Liu, C.Z., 2010. Magnetic mesoporous silica nanoparticles: Fabrication and their laccase immobilization performance. *Bioresour. Technol.* 101 (23), 8931–8935. <http://dx.doi.org/10.1016/j.biortech.2010.06.115>.
- Wang, P., Ma, J., Wang, L., Li, L., Yan, X., Zhang, R., Cernava, T., Jin, D., 2023. Di-n-butyl phthalate stress induces in the core bacterial community associated with nitrogen conversion during agricultural waste composting. *J. Hard Mater.* 446, 130695. <http://dx.doi.org/10.1016/j.jhazmat.2022.130695>.
- Wang, H., Zhao, X., Wang, S., Tao, S., Ai, N., Wang, Y., 2015. Fabrication of enzyme-immobilized halloysite nanotubes for affinity enrichment of lipase inhibitors from complex mixture. *J. Chromatogr. A* 1392, 20–27. <http://dx.doi.org/10.1016/j.chroma.2015.03.002>.
- Yeniöva-Erpek, C.E., Özkoc, G., Yilmazer, U., 2015. Effects of halloysite nanotubes on the performance of plasticized poly(lactic acid)-based composite. *Polym. Compos.* 37 (11), 3134–3148. <http://dx.doi.org/10.1002/pc.23511>.
- You, Z., Bedrikovetsky, P., Badalyan, A., Hand, M., 2015. Particle immobilization in porous media: Temperature effects on competing electrostatic and drag forces. *Geophys. Res. Lett.* 42 (8), 2852–2860. <http://dx.doi.org/10.1002/2015GL063986>.
- Zhai, R., Zhang, B., Liu, L., Xie, Y., Zhang, Y., Liu, J., 2010. Immobilization of enzyme biocatalyst on natural halloysite nanotube. *Cataly. Commun.* 12, 259–263. <http://dx.doi.org/10.1016/j.catcom.2010.09.030>.
- Zhai, R., Zhang, B., Wan, Y., Li, C., Wang, J., Liu, J., 2013. Chitosan-halloysite hybrid nanotubes: Horseradish peroxidase immobilization and applications in phenol removal. *Chem. Eng. J.* 214, 304–309. <http://dx.doi.org/10.1016/j.cej.2012.10.073>.
- Zhang, X.Y., Fan, X., Qiu, Y.J., Li, C.Y., Xing, S., Zheng, Y.T., Xu, J.H., 2014. Newly identified thermostable esterase from *Sulfobacillus acidophilus*: Properties and performance in phthalate ester degradation. *Appl. Environ. Microbiol.* 80 (22), 6870–6878. <http://dx.doi.org/10.1128/AEM.02072-14>.
- Zhao, W.W., Xu, J.J., Chen, H.Y., 2017. Photoelectrochemical enzymatic biosensors. *Biosens. Bioelectron.* 92, 294–304. <http://dx.doi.org/10.1016/j.bios.2016.11.009>.